



Polarization of the Ly α Lines of H I and He II as a Tool for Exploring the Solar Corona

Supriya Hebbur Dayananda^{1,2} , Javier Trujillo Bueno^{1,2,3} , Ángel de Vicente^{1,2} , and Tanausú del Pino Alemán^{1,2} ¹Instituto de Astrofísica de Canarias, E-38205, La Laguna, Tenerife, Spain; supriya@iac.es²Departamento de Astrofísica, Universidad de La Laguna, 38206 La Laguna, Tenerife, Spain³Consejo Superior de Investigaciones Científicas, Spain

Received 2021 June 10; revised 2021 June 29; accepted 2021 June 29; published 2021 October 22

Abstract

The near-Earth space weather is driven by the quick release of magnetic free energy in the solar corona. Probing this extremely hot and rarified region of the extended solar atmosphere requires modeling the polarization of forbidden and permitted coronal lines. To this end, it is important to develop efficient codes to calculate the Stokes profiles that emerge from given three-dimensional (3D) coronal models and this should be done taking into account the symmetry breaking produced by the presence of magnetic fields and non-radial solar wind velocities. We have developed such a tool with the aim of theoretically predicting and interpreting spectropolarimetric observations of the solar corona in permitted and forbidden lines. In this paper, we show the results of a theoretical investigation of the linear polarization signals produced by scattering processes in the H I Ly α line at 1216 Å and in the He II Ly α line at 304 Å using 3D coronal models by Predictive Science Inc. These spectral lines have very different critical magnetic fields for the onset of the Hanle effect (53 G and 850 G, respectively), as well as different sensitivities to the Doppler effect caused by the solar wind velocities. We study under which circumstances simultaneous observations of the scattering polarization in these Ly α lines can facilitate the determination of magnetic fields and macroscopic velocities in the solar corona.

Unified Astronomy Thesaurus concepts: [Solar corona \(1483\)](#); [Solar magnetic fields \(1503\)](#); [Solar coronal lines \(2038\)](#); [Solar wind \(1872\)](#); [Solar physics \(1476\)](#)

1. Introduction

There are two types of spectral lines that encode information on the 10^6 K plasma of the solar corona: forbidden lines at visible and infrared (IR) wavelengths and permitted lines in the ultraviolet (UV) spectral region. The polarization that some physical mechanisms introduce in such spectral lines is sensitive to the magnetic fields of the solar corona (e.g., the reviews by Casini et al. 2017; Trujillo Bueno et al. 2017). These physical mechanisms are the scattering of anisotropic radiation coming from the underlying solar disk and the Hanle and Zeeman effects (see Landi Degl’Innocenti & Landolfi 2004). The circular polarization signals are dominated by the Zeeman effect, but they are very hard or impossible to measure because their amplitudes $\sim \frac{\lambda B}{\sqrt{T}}$, λ being the spectral line wavelength and T and B the temperature and magnetic field strength of the coronal plasma, respectively. The linear polarization signals are caused by scattering processes and in the presence of a magnetic field inclined with respect to the symmetry axis of the incident radiation field, they are modified by the Hanle effect. The critical magnetic field strength (B_H) for the onset of the Hanle effect in a spectral line is inversely proportional to the lifetime of the line’s upper level. For the typical magnetic field strengths (B) expected in the solar corona, the forbidden lines are in the saturation regime of the Hanle effect (i.e., their linear polarization is sensitive only to the magnetic field orientation, because $B \gg 5B_H$), while the permitted lines are in the unsaturated regime (i.e., their linear polarization is sensitive to both the orientation and the strength of the coronal magnetic field, because typically $0.2B_H \lesssim B \lesssim 5B_H$). In the present paper, we focus on the linear polarization produced by scattering processes in two permitted lines of the solar ultraviolet spectrum, which have very different sensitivities to the Hanle effect.

One of the spectral lines considered here is the hydrogen Ly α line at 1216 Å, whose critical magnetic field strength for the onset of the Hanle effect is $B_H \approx 53$ G. This spectral line originates all through the upper chromosphere and it shows a broad intensity profile in emission with a small depression at its core (e.g., Warren et al. 1998). The residual neutral hydrogen atoms in the solar corona scatter the intense Ly α line radiation coming from the underlying chromosphere (Gabriel et al. 1971; Moses et al. 2020). At coronal heights, the anisotropy of the Ly α emission line radiation coming from the solar chromosphere is substantial. Consequently, the scattered coronal Ly α radiation is expected to be linearly polarized. In the idealized situation of a spherically symmetric and static solar atmosphere, the linear polarization of the scattered radiation is parallel to the solar limb. In the presence of a non-radial magnetic field in the (optically thin) corona of such an idealized solar atmosphere the radiation field coming from the underlying solar disk still has axial symmetry around the radial direction, but the Hanle effect caused by the inclined magnetic field modifies the linear polarization of the zero-field case (Bommier & Sahal-Brechot 1982; Fineschi et al. 1992). However, the Hanle effect is not the only mechanism capable of modifying the linear polarization produced by scattering in permitted lines like hydrogen Ly α (e.g., chapter 12 of Landi Degl’Innocenti & Landolfi 2004 and references therein). Of particular importance is the Doppler effect caused by the solar wind velocity, which has to be taken into account because at the UV wavelengths of the permitted lines the intensity of the solar-disk radiation has spectral structure (e.g., an emission profile for the Ly α line of H I). At each point in the solar corona, its rarefied plasma is moving with a macroscopic velocity, with the implication that the mean intensity (J_0^0) of the radiation field as seen in the comoving frame increases (decreases) with increasing velocity for the case of an incident

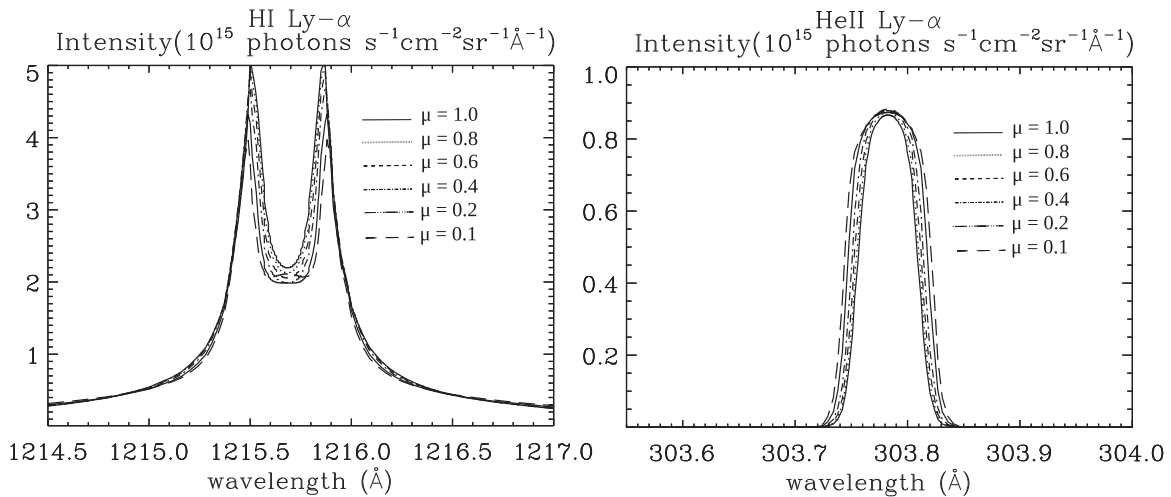


Figure 1. Center-to-limb variation of the intensity profiles of the Ly α lines of H I (left panel) and He II (right panel), calculated in the FAL-C solar semi-empirical model. The LOS is characterized by $\mu = \cos\theta$, with θ the heliocentric angle.

radiation field with an absorption (emission) line. In addition to this well-known Doppler brightening (dimming) effect, the anisotropy of the incident radiation field in the comoving reference frame is modified depending on the modulus and inclination of the macroscopic velocity with respect to the solar radial direction. Moreover, at points in the solar corona where the macroscopic velocity of the plasma is non-radial, we may have a symmetry breaking because the radiation coming from different points of the underlying solar disk with the same line-of-sight (LOS) inclination is differently affected by the Doppler effect (Sahal-Brechot et al. 1986, 1998; Khan et al. 2011; Khan & Landi Degl’Innocenti 2012).

The other spectral line investigated here is the Ly α line of He II at 304 Å, whose critical magnetic field for the onset of the Hanle effect is $B_H \approx 850$ G (Trujillo Bueno et al. 2012). This spectral line originates in the chromosphere–corona transition region (TR) and it shows an intensity profile in emission, which is narrower than that of the hydrogen Ly α line (Doscsek et al. 1974; Cushman et al. 1975; Cushman & Rense 1978). There are residual He II ions in the solar corona, which scatter the He II 304 Å line radiation coming from the underlying TR (Gabriel et al. 1995; Moses et al. 2020). At coronal heights the anisotropy of this spectral line radiation is substantial, and we therefore expect that the scattered coronal Ly α line of He II at 304 Å is also linearly polarized. However, in contrast with the case of the hydrogen Ly α line, we expect that the Ly α line of He II is rather insensitive to the weak magnetic fields of the solar corona (because $B_H \approx 850$ G for the He II line), but much more sensitive to the solar wind velocities (because of the much narrower He II emission line radiation coming from the TR).

In this paper we consider state-of-the-art three-dimensional (3D) models of the solar corona and calculate the maps of the linear polarization signals produced by scattering in the Ly α lines of H I and He II, taking into account and neglecting the magnetic field and macroscopic velocity of the coronal models. Our aim is to quantitatively investigate whether the different sensitivities of this pair of Ly α lines to the coronal magnetic field and to the solar wind outflows can be exploited for facilitating the diagnostics of these quantities. To the best of our knowledge, this is the first time that the scattering polarization of the Ly α line of He II produced by the residual He II ions of solar coronal models is investigated. The works of

Trujillo Bueno et al. (2012) and Belluzzi et al. (2012) concerned the linear polarization of the Ly α lines of H I and He II produced by scattering in the upper solar chromosphere and in the TR, which required taking into account the effects of radiative transfer. A different line pair that has been proposed for coronal magnetometry is hydrogen Ly α and the 10830 Å multiplet of neutral helium (see Raouafi et al. 2016).

In Section 2 we describe the formulation of the problem. In Section 3 we discuss some of the theoretical results, emphasizing the importance of velocity fields in understanding the linear polarization signals of the Ly α lines of H I and He II in the solar corona. Furthermore, in Section 4 we describe the two 3D Predictive Science Inc. models we have chosen and the emergent Stokes profiles calculated, taking into account both the velocity and magnetic field of the models under consideration. Finally, we present our conclusions in Section 5.

2. Formulation of the Problem

A detailed review of the physics of the spectral line polarization that results from the resonance scattering of solar-disk photons by residual coronal atoms (e.g., of H I or He II) can be found in Section 3 of Trujillo Bueno et al. (2017). Here we summarize the main physical ingredients of the problem’s formulation. Both Ly α lines result from the transitions between levels $n = 1$ and $n = 2$, with n being the principal quantum number. The $n = 1$ ground level is composed of the singlet $1s^2S_{1/2}$, while the upper level $n = 2$ consists of the singlet $2s^2S_{1/2}$ and the doublet $2p^2P_{1/2,3/2}$. In both Ly α lines, the radiation observed in the solar corona is dominated by resonance fluorescence (Gabriel et al. 1971, 1995; Patchett et al. 1981; Raymond et al. 1997; Moses et al. 2020). Since collisional processes are expected to be negligible in the formation of these Ly α lines in the solar corona, the upper level $2s^2S_{1/2}$ cannot be populated and it can be ignored.⁴ The fact that the separation between the $2p^2P_{1/2}$ and $2p^2P_{3/2}$ fine structure (FS) upper levels is about 17 times larger than their natural width implies that in a weakly magnetized and optically thin medium like the solar corona we

⁴ We are also assuming that electric fields in the solar corona do not play any role on the excitation of this level (see Favati et al. 1987; Casini 2005, for information on the possible impact of an electric field).

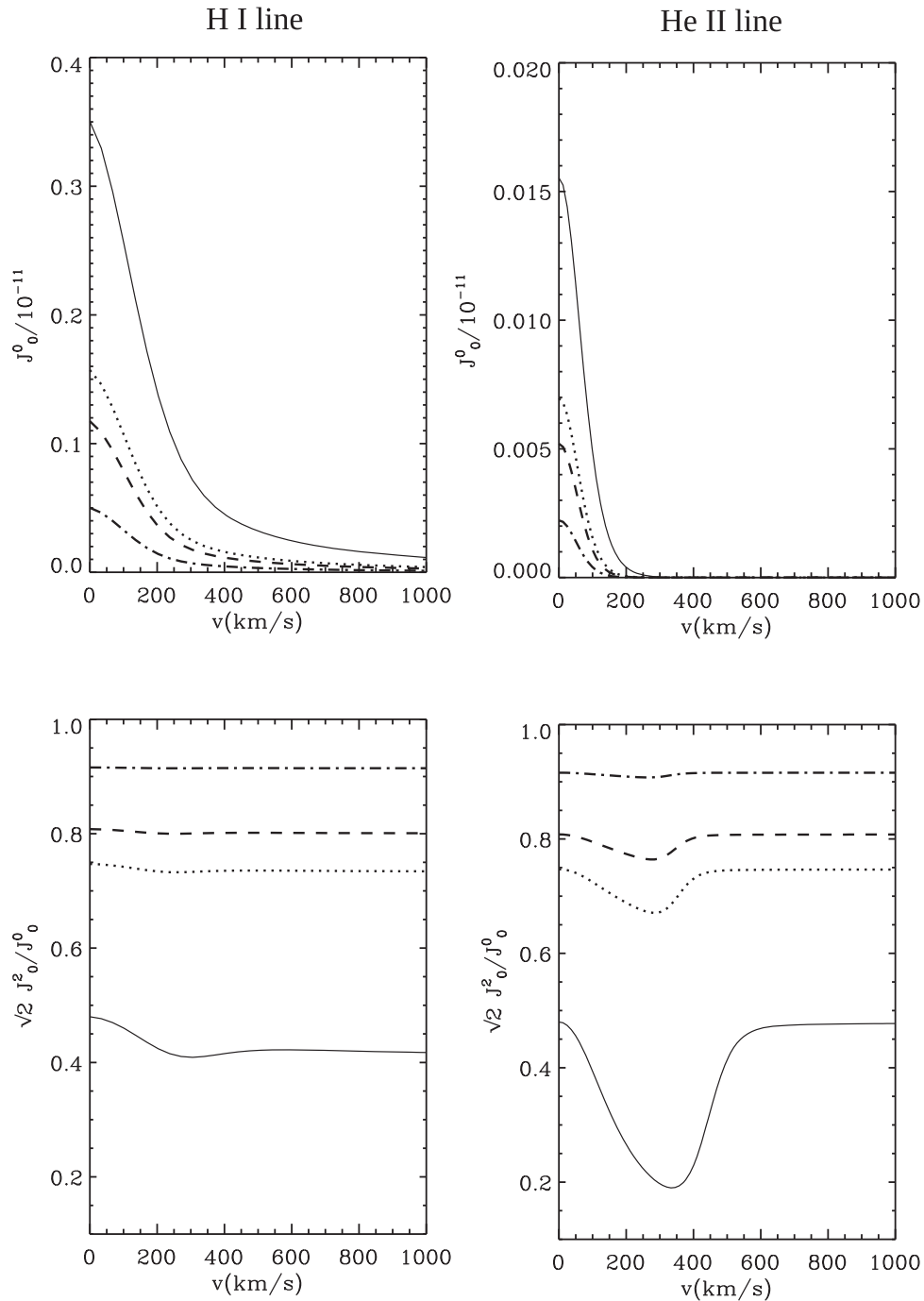


Figure 2. Variation of the indicated components of the comoving frame radiation field tensor with the velocity of the assumed radial solar wind, for the H I Ly α line (left panels) and the He II Ly α line (right panels). The different curves correspond to the following heights above the solar visible disk: solid $h = 0.25 R_\odot$, dotted $h = 0.75 R_\odot$, dashed $h = 1.0 R_\odot$, and dotted-dashed $h = 2.0 R_\odot$.

can safely neglect any quantum mechanical interference between the magnetic sublevels pertaining to these two upper levels. Both Ly α lines result from two transitions between the $1s^2S_{1/2}$ lower level and the $2p^2P_{1/2}$ and $2p^2P_{3/2}$ upper levels, which are blended because their separation is much smaller than the line's Doppler width. Although the only level that contributes to the scattering polarization in these Ly α lines is the upper level with angular momentum $J = 3/2$, the FS of the Ly α lines must, however, be taken into account because it reduces the polarizability factor of the lines. Fortunately, as shown by Bommier & Sahal-Brechot (1982), the hyperfine

structure can be safely neglected for modeling the scattering polarization of Ly α in the solar corona. In summary, a reliable modeling of the Ly α radiation scattered by the solar corona can be achieved by means of a three-level model atom with the $1s^2S_{1/2}$ ground level and the $2p^2P_{1/2}$ and $2p^2P_{3/2}$ upper levels, without any quantum interference between them.

The linear polarization produced by the scattering of anisotropic radiation in both Ly α lines is sensitive to magnetic fields with strengths between $0.2B_H$ and $5B_H$, approximately, where $B_H = 1.137 \times 10^{-7}/(t_{\text{lifeg}})$ is the critical magnetic strength for the onset of the Hanle effect (with t_{lifeg} and

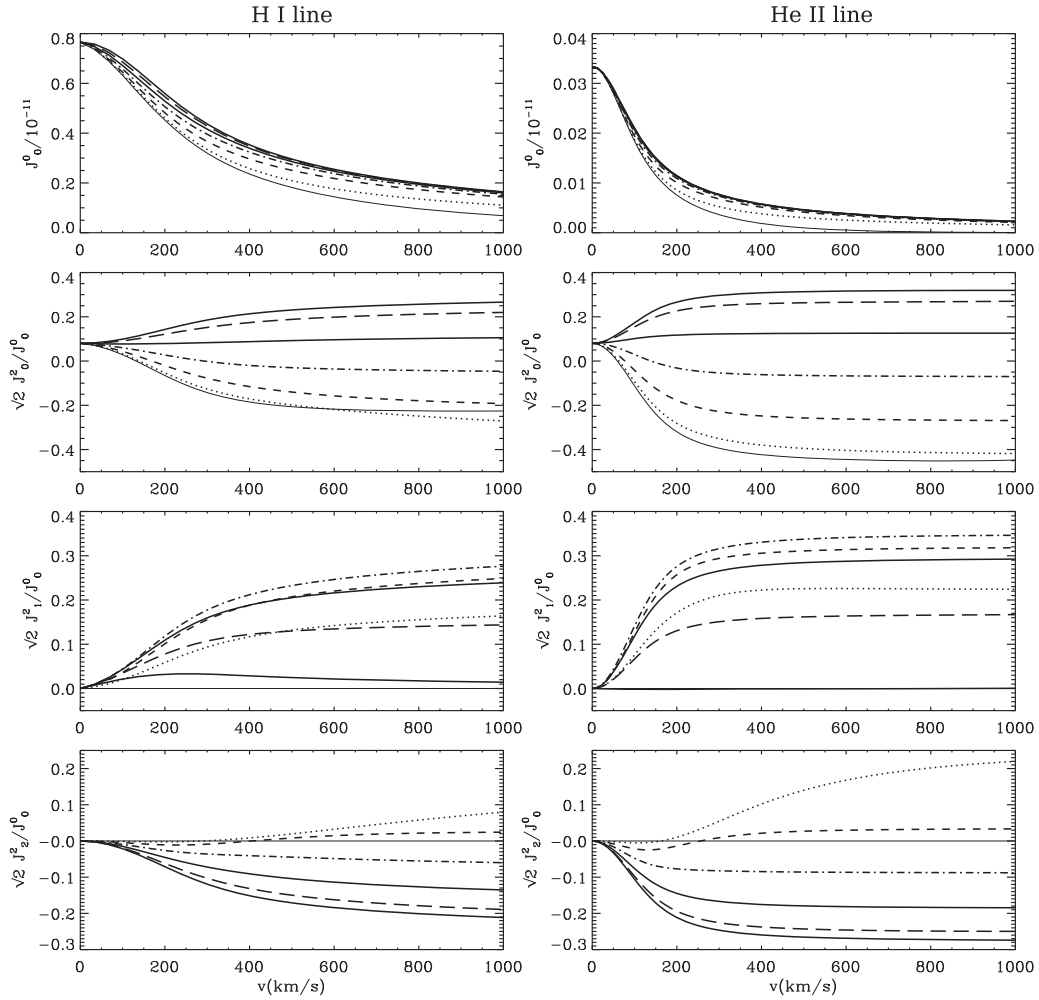


Figure 3. The impact of non-radial solar wind velocities on the radiation field tensors for the H I Ly α line (left panels) and the He II Ly α line (right panels) at a height $h = 0.01 R_{\odot}$ above the solar surface. The various curves are for the following inclinations of macroscopic velocity: thin solid-0°; dotted-15°; dashed-30°; dotted-dashed-45°; dashed-triple-dotted-60°; long dashed-75°; thick solid-90°. For all curves, the azimuth angle of the velocity is 0°. We show only the real components of J_1^2 and J_2^2 because their imaginary components are very small for the chosen azimuth.

$g = 4/3$ the radiative lifetime in seconds and the Landé factor of the line’s upper level with $J = 3/2$, respectively). While $B_H \approx 53$ G for the hydrogen Ly α line at 1216 Å, it is $B_H \approx 850$ G for the Ly α line of He II at 304 Å (Trujillo Bueno et al. 2012). This is because $t_{\text{life}} \approx 1/A_{ul}$, and the Einstein coefficient A_{ul} for spontaneous emission from the upper (u) to the lower (l) level for the Ly α line of H I at 1216 Å is $A_{ul} \approx 6.264 \times 10^8 \text{ s}^{-1}$ and is $A_{ul} \approx 1.0029 \times 10^{10} \text{ s}^{-1}$ for the He II line at 304 Å, which is 16 times larger than the former.

To model the polarization of solar coronal lines, we have developed a computer code based on the multilevel atom theory described in Section 7.2 of Landi Degl’Innocenti & Landolfi (2004). Our choice for the quantization axis for total angular momentum is the solar radius vector through the considered spatial point in the solar corona; therefore, the statistical equilibrium equations are Equations (7.78) given in this monograph, which can be directly solved once the incident radiation field is specified for each radiative transition in the multilevel model under consideration. The numerical solution of these equations gives the multipolar components $\rho_Q^K(J)$ of the atomic density matrix for each atomic level of total angular momentum J . Since the solar corona is optically thin at the wavelengths of the considered Ly α lines, we only have to

calculate the emission coefficient $\epsilon_i(\nu, \Omega)$ (where the index “ i ” take the values 0,1,2, and 3, corresponding to Stokes I , Q , U , and V , respectively) for each line frequency ν and propagation direction Ω . This emission coefficient in the four Stokes parameters $I_i(\nu, \Omega)$ has to be calculated at each position along the considered off-limb LOS, and we finally obtain the frequency-integrated Stokes signal

$$I_i(\Omega) = \int d\nu \int_{\text{LOS}} \epsilon_i(\nu, \Omega) ds, \quad (1)$$

where s is the geometrical distance along the LOS.

The emission coefficient depends on the multipolar components $\rho_Q^K(J_u)$ of the atomic density matrix of the upper levels of the Ly α lines, the calculation of which requires solving the statistical equilibrium equations for the three-level model atom mentioned above. Given that J -state interference does not play any role here and that collisional processes are negligible, the two upper levels are not coupled and one is basically left with a pair of two-level atom equations for the two blended transitions. The crucial quantity that enters these equations is the radiation field tensor J_Q^K , which quantifies the symmetry properties of the Ly α radiation that illuminates the H I and He II

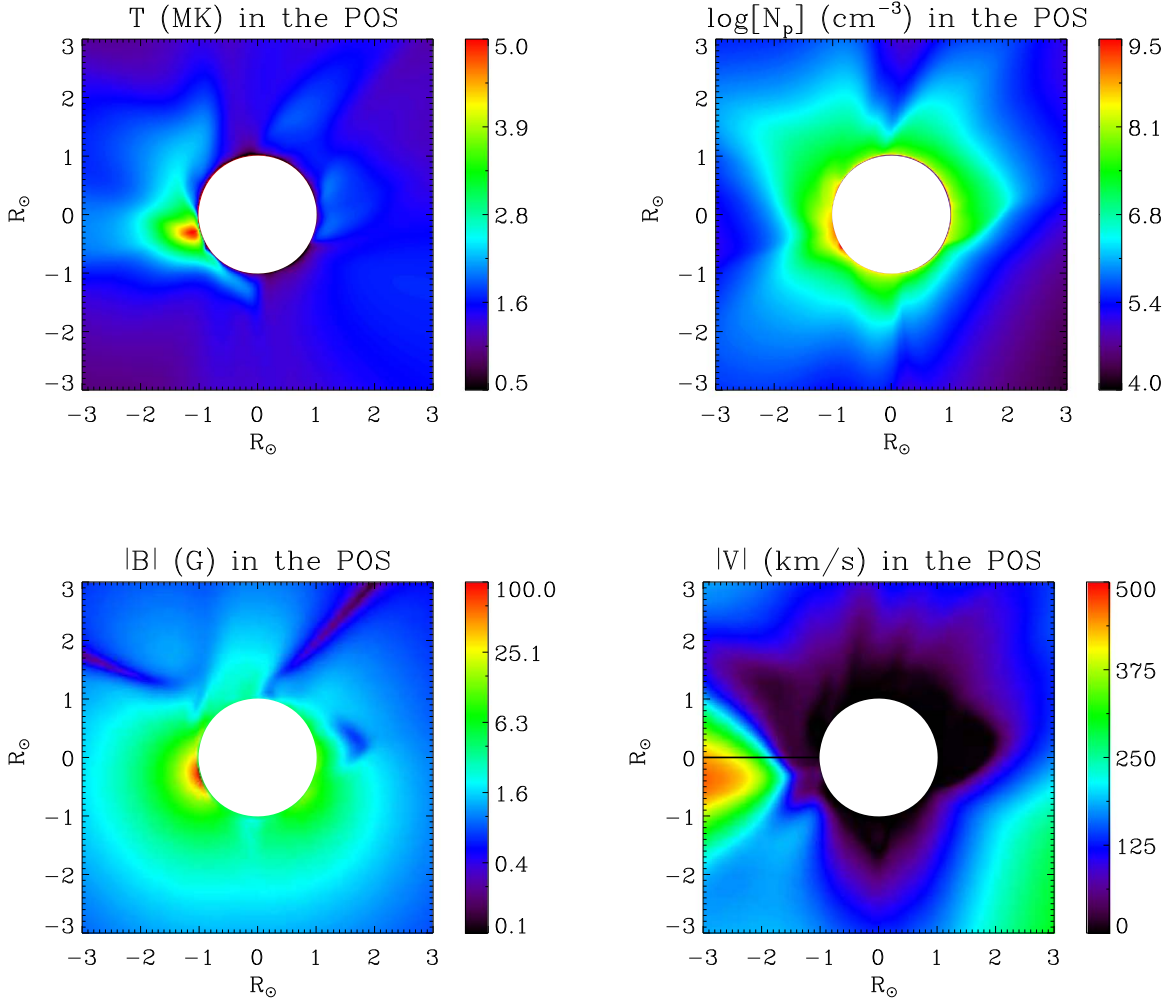


Figure 4. Temperature, proton number density, magnetic field strength, and modulus of the macroscopic velocity for “the magnetic model” CR2157 in the POS. The solid line in the bottom right panel indicates the direction across which the variation of different quantities for this model is given in Figures 6, 8, and 12.

atoms of the solar corona:

$$J_Q^K(\nu_0) = \int_{-\infty}^{\infty} f(\mathbf{v} - \mathbf{w}) d^3\mathbf{v} \times \oint \frac{d\Omega'}{4\pi} T_Q^K(0, \Omega') I\left(\nu_0 \left(1 + \frac{\mathbf{v} \cdot \Omega'}{c}\right), \Omega'\right), \quad (2)$$

where ν_0 is the transition frequency, \mathbf{v} is the vector sum of the thermal velocity and of the solar wind velocity, \mathbf{w} , and $f(\mathbf{v} - \mathbf{w})$ is the velocity distribution function of the atoms in the corona. $T_Q^K(0, \Omega')$ is the polarization tensor, which depends on the propagation direction $\Omega'(\theta', \chi')$ of the incoming radiation (see Figure 12.10 in LL04; $\Omega(\theta, \chi)$ in this figure corresponds to $\Omega'(\theta', \chi')$). The last term in Equation (2) represents the Stokes I emission profile of the incoming Ly α radiation, which is Doppler shifted as seen by the coronal atoms. This equation accounts for the loss of axial symmetry of the radiation field at any given point in the solar corona, due to the Doppler effect caused by the macroscopic velocity of the solar wind.

In Equation (2) the term of the Doppler effect is

$$\mathbf{v} \cdot \Omega' = v [\cos \theta' \cos \theta_v + \sin \theta' \sin \theta_v \cos(\chi' - \chi_v)], \quad (3)$$

where v is the modulus of the velocity and the θ_v and χ_v angles indicate its direction. In a reference frame at rest with respect to

the solar surface and having the Z -axis directed along the solar radius vector through the considered point in the solar corona, the radiation coming from the underlying solar disk is cylindrically symmetrical (i.e., independent of the azimuth), which implies that the only non-zero components of the radiation field tensor are J_0^0 (mean intensity) and J_0^2 (anisotropy). However, if the solar wind velocity has non-radial components, an observer in the comoving frame (i.e., the reference system moving with velocity \mathbf{v} at the point under consideration) will see a radiation intensity that depends on the azimuth, which also implies that the J_1^2 and J_2^2 components will be non-zero. Clearly, in the case of a purely radial solar wind, $J_1^2 = J_2^2 = 0$. However, J_0^0 and J_0^2 are modified with respect to the static case because, due to the Doppler effect, the coronal atoms experience a lower radiation intensity (correspondingly, the coronal atoms would experience Doppler brightening if the incoming radiation were an absorption instead of an emission profile; see chapter 12 of Landi Degl’Innocenti & Landolfi 2004, for more details).

The following section shows some illustrative results useful to clarify how the various components of the (comoving frame) radiation field tensor of the Ly α lines of H I and He II react to radial and non-radial solar wind macroscopic motions. These academic results will be helpful in better understanding the

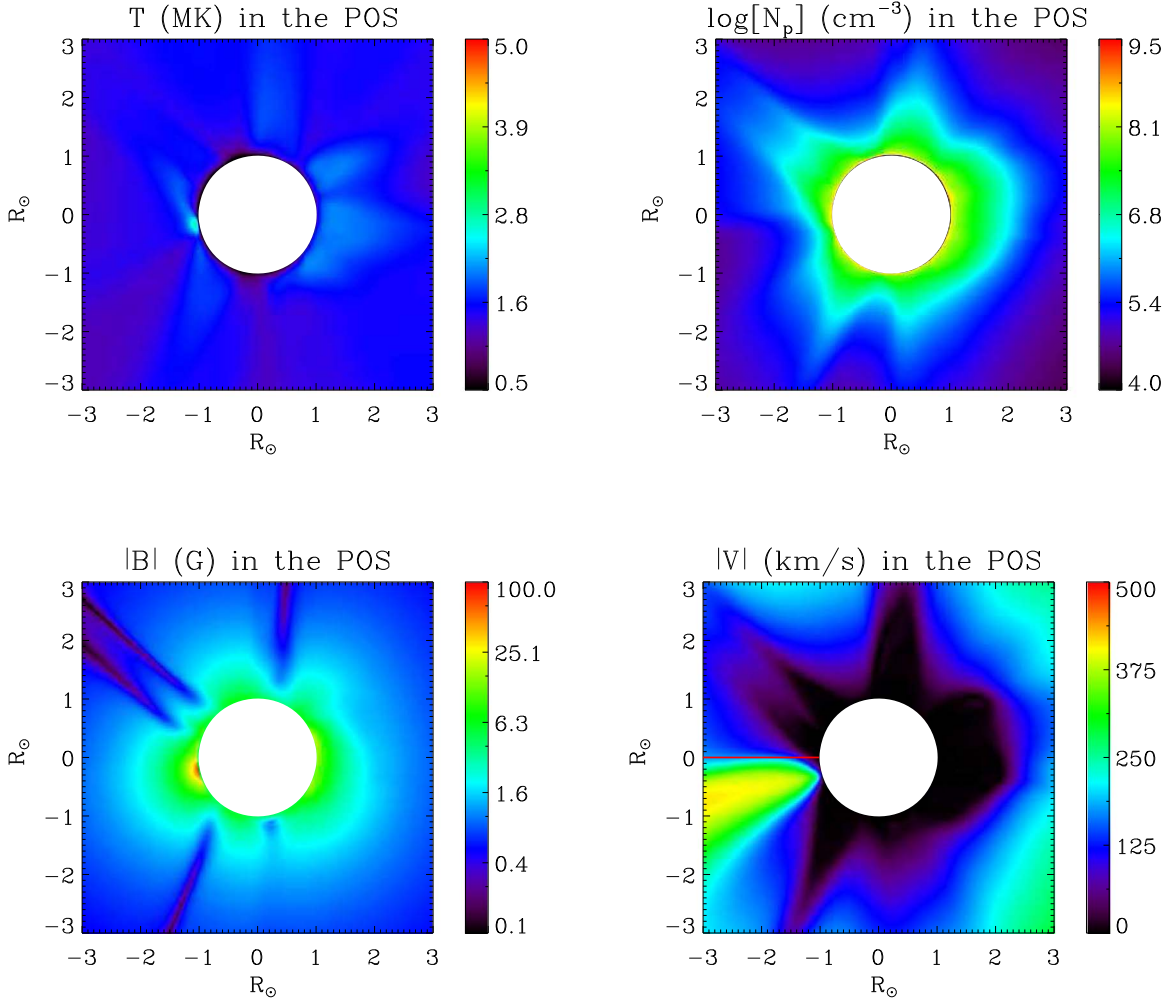


Figure 5. Temperature, proton number density, magnetic field strength, and modulus of the macroscopic velocity for “the dynamic model” CR2138 in the POS. The solid line in the bottom right panel indicates the direction across which the variation of different quantities for this model is given in Figures 6, 8, and 12.

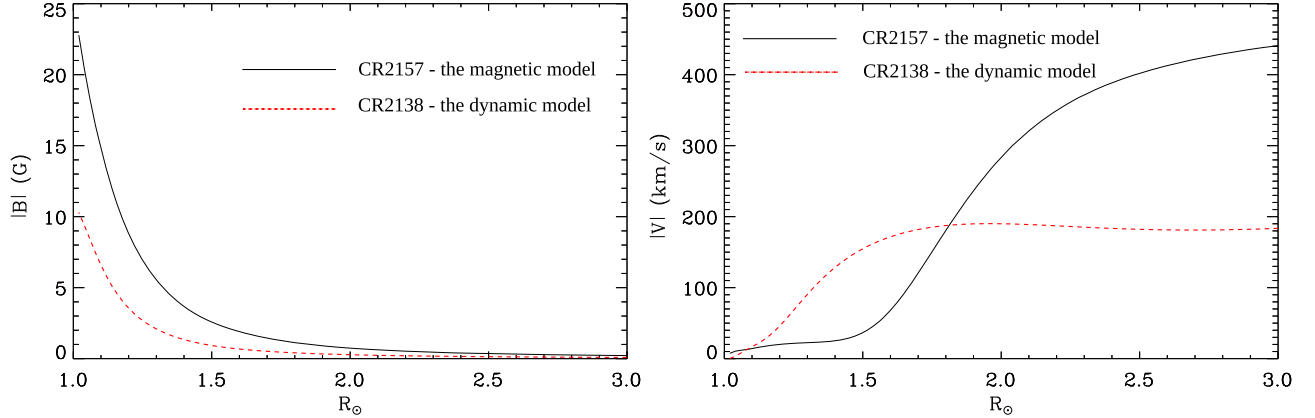


Figure 6. Variation of the model’s magnetic field strength and modulus of the velocity along the radial direction indicated in Figures 4 and 5.

results of Section 4, where we show the maps of the linear polarization signals in both $\text{Ly}\alpha$ lines produced by scattering in 3D solar coronal models from Predictive Science Inc. In the calculations of this paper, the intensity profiles of the corresponding $\text{Ly}\alpha$ line radiation that emerges from the quiet solar disk are given in Figure 1. These Stokes I profiles result from non-equilibrium radiative transfer calculations with the RH code of Uitenbroek (2001) in the semi-empirical model C

of Fontenla et al. (1993, hereafter, FAL-C). The radiation at the H I $\text{Ly}\alpha$ line is calculated for a 10 level (9 H I levels + H II) model atom without fine structure, taking into account partial frequency redistribution effects in both $\text{Ly}\alpha$ and $\text{Ly}\beta$ transitions. The radiation at the He II $\text{Ly}\alpha$ line is calculated for a 53 level (46 He I levels + 6 He II levels + He III) model atom with fine structure only in the He I atomic levels and taking into account partial frequency redistribution effects in

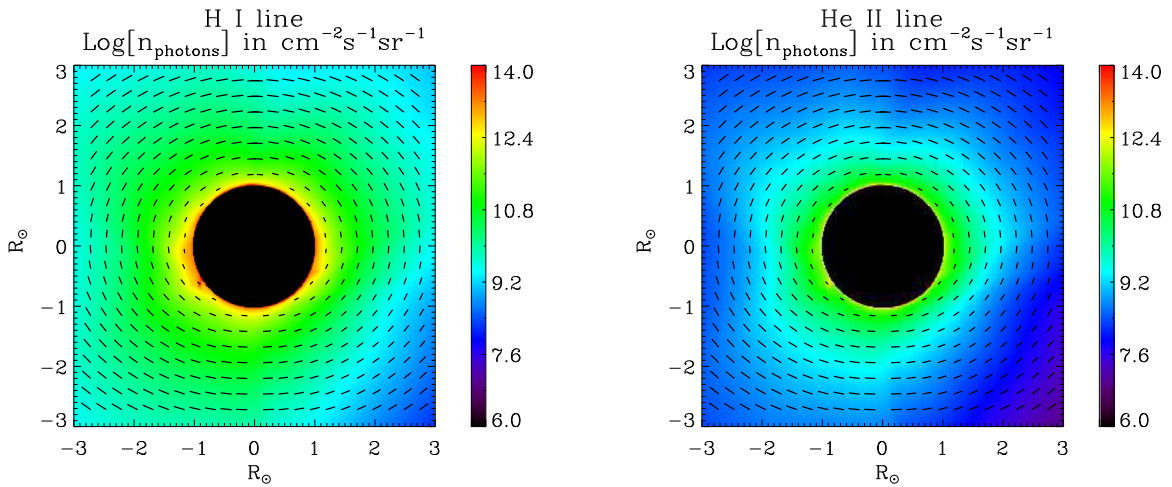


Figure 7. The intensity of the Ly α lines of H I (left panel) and He II (right panel) computed in “the magnetic model” CR2157 without its magnetic field and macroscopic velocity, including the LOS integration. The black short lines indicate the direction of the linear polarization and their length the amplitude of the polarization signals.

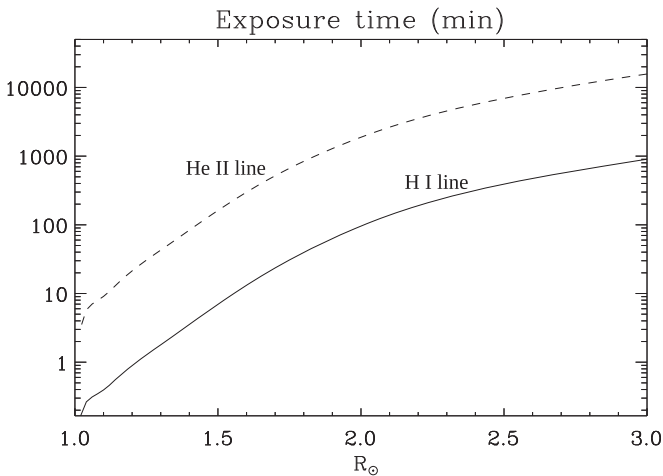


Figure 8. Required exposure time for the Ly α lines of H I and He II along the radial direction computed for a set of parameters specified in the text.

the He II Ly α line. Both atomic models are part of the RH code, but we have modified them to increase the number of frequency nodes (in particular, the relevant Ly α transitions are sampled with 200 frequency nodes) and to account for partial redistribution effects in the He II Ly α line. As seen in Figure 1, the center-to-limb variation of these intensity profiles is not very significant. At coronal heights, the anisotropy of the spectral line radiation in both Ly α lines is fully dominated by the fact that the larger the height above the visible solar-disk sphere, the smaller the solid angle subtended. We have accounted for this fact as explained in Section 12.3 of Landi Degl’Innocenti & Landolfi (2004).

3. Doppler Dimming and Symmetry Breaking

It is of interest to start illustrating the impact of radial and non-radial solar wind velocities on the comoving frame radiation field tensor (cf., Landi Degl’Innocenti & Landolfi 2004). To this end, we assume a 10^6 K isothermal solar coronal model with a constant outward macroscopic velocity and calculate the components of the radiation field tensor for the Ly α lines of H I and He II. As shown in Figure 1, the intensity profiles of the Ly α line radiation coming from the

underlying solar disk have very different widths, with the H I 1216 Å line being ~ 8.5 times broader than the He II 304 Å line.

First, we consider a range of solar wind velocities (0 – 1000 km s $^{-1}$) directed along the solar radius and calculate the radiation field tensor at various heights above the Sun’s visible disk. Given that the macroscopic velocity is radial and that the underlying solar disk is assumed to be devoid of any structure (e.g., sunspots) capable of breaking the axial symmetry of the incident radiation field, the only non-zero components of the radiation field tensor are J_0^0 and J_0^2 . Figure 2 shows the results for the Ly α lines of H I (left panels) and He II (right panels), namely J_0^0 (upper panels) and $\sqrt{2}J_0^2/J_0^0$ (bottom panels) against the modulus of the radial solar wind velocity. We recall that the anisotropy factor of the radiation field at the spatial point under consideration is $\sqrt{2}J_0^2/J_0^0$, which is unity for the case of a unidirectional unpolarized radiation beam.

As expected, the mean intensity J_0^0 is larger for the H I line, because for this spectral line the intensity that emerges from the underlying solar disk is about one order of magnitude larger than that corresponding to the He II line. Also, the larger the height above the solar visible disk, the smaller the mean intensity because the solid angle subtended by the Sun’s visible sphere decreases. The most noteworthy point is the rapid decrease of J_0^0 as the macroscopic velocity of the assumed radial solar wind increases. This so-called Doppler-dimming effect occurs because due to the Doppler effect, the emission peak of the radiation that comes from the underlying chromosphere and transition region, as seen from the coronal atoms, falls out of resonance. As a result, for sufficiently large velocities, the solar wind atoms see, at frequency ν_0 , the radiation emitted by the underlying solar disk in the far wings of the line, where the intensity of the Ly α line under consideration is smaller than at the line center. As expected, the Ly α line of He II is more sensitive to this Doppler-dimming effect because the intensity profile of the incoming radiation is narrower.

As seen in the bottom panels of Figure 2, in the static case, the anisotropy factor of both Ly α lines is exactly the same simply because the two lines have the same polarizability factor. When the solar coronal plasma is moving radially, the anisotropy factor first decreases and then grows as the magnitude of the velocity increases. The decrease occurs

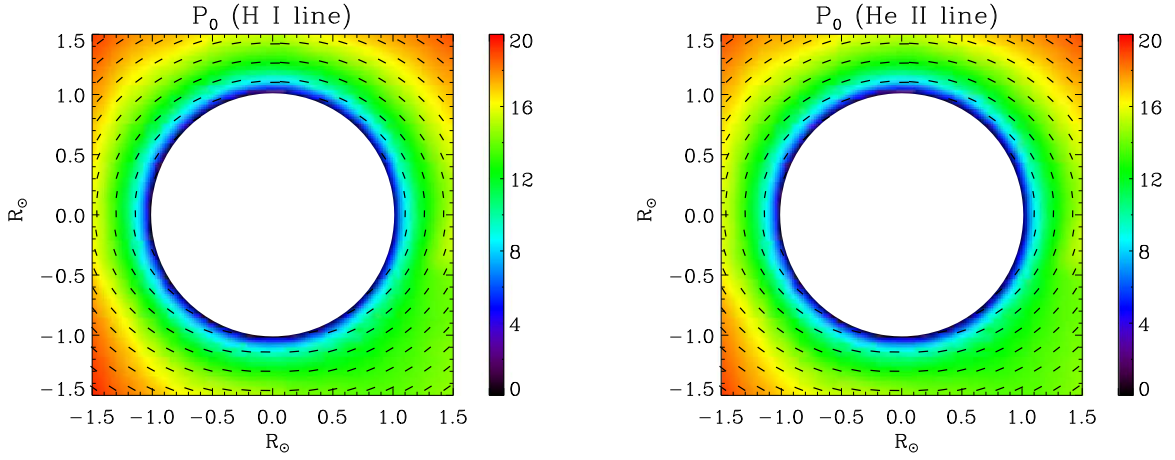


Figure 9. The fractional total linear polarization of the Ly α lines of H I (left panel) and He II (right panel) computed in “the magnetic model” CR2157 without its magnetic field and macroscopic velocity, including the LOS integration. Like in Figure 7, the black short lines indicate the direction of the linear polarization and their length the amplitude of the polarization signals.

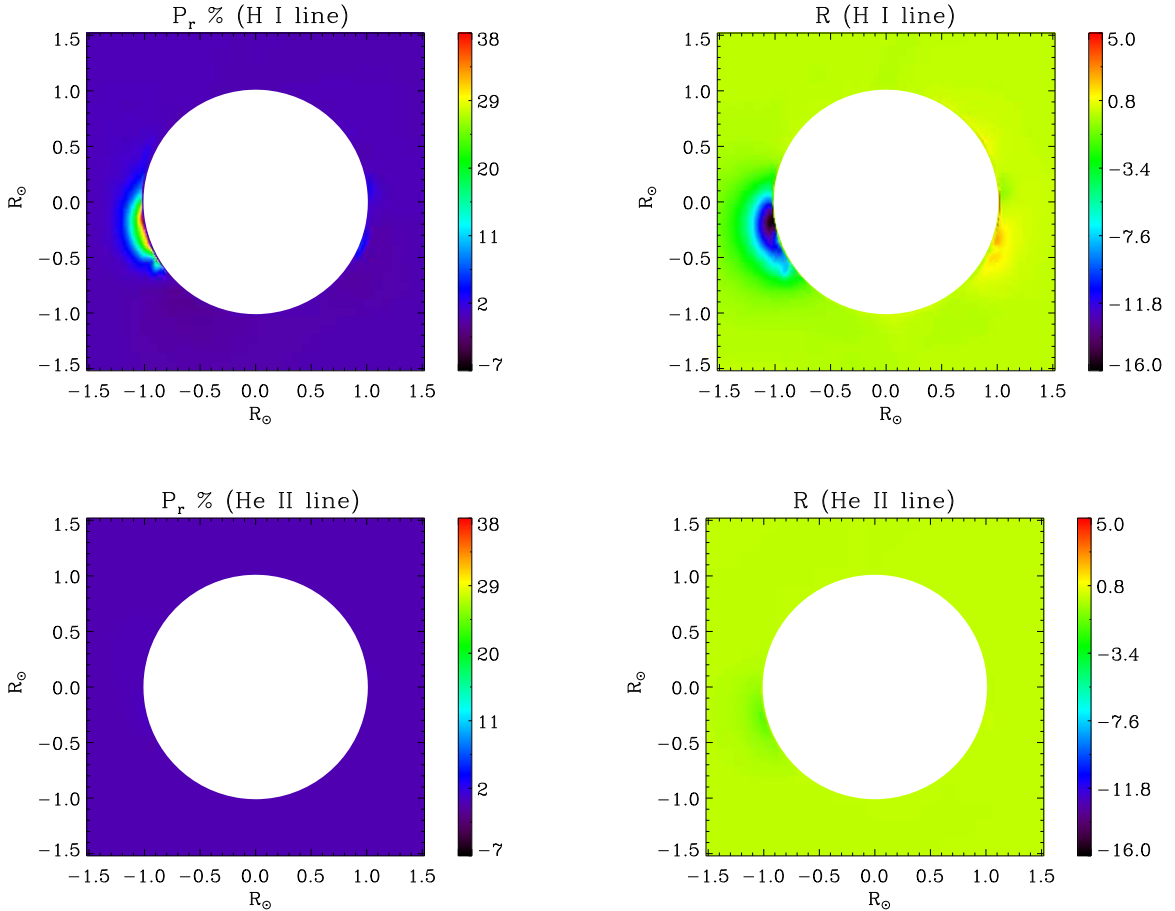


Figure 10. The relative polarization P_r and the rotation angle R of the polarization plane of the Ly α lines of H I (top panels) and the He II (bottom panels) calculated in “the magnetic model” CR2157 taking into account the Hanle effect but ignoring the model’s macroscopic velocity.

because the Doppler effect acts as a limb brightening: the nearly radial beams of the incoming radiation are redshifted and hence the coronal atoms see less intensity at frequency ν_0 , while the same effect is weaker for the predominantly horizontal radiation beams. Clearly, as soon as the velocity is sufficiently large, the anisotropy factor tends to its static value because the coronal atoms see at frequency ν_0 , the radiation

emitted by the solar disk in the far wings of the line. This occurs much sooner for the narrower Ly α line of He II; therefore, the anisotropy factor in both lines is not exactly the same for 1000 km s^{-1} . Also, the sensitivity of the comoving frame anisotropy factor to the radial velocity is larger for the Ly α line of He II because the intensity profile of its incoming radiation is narrower.

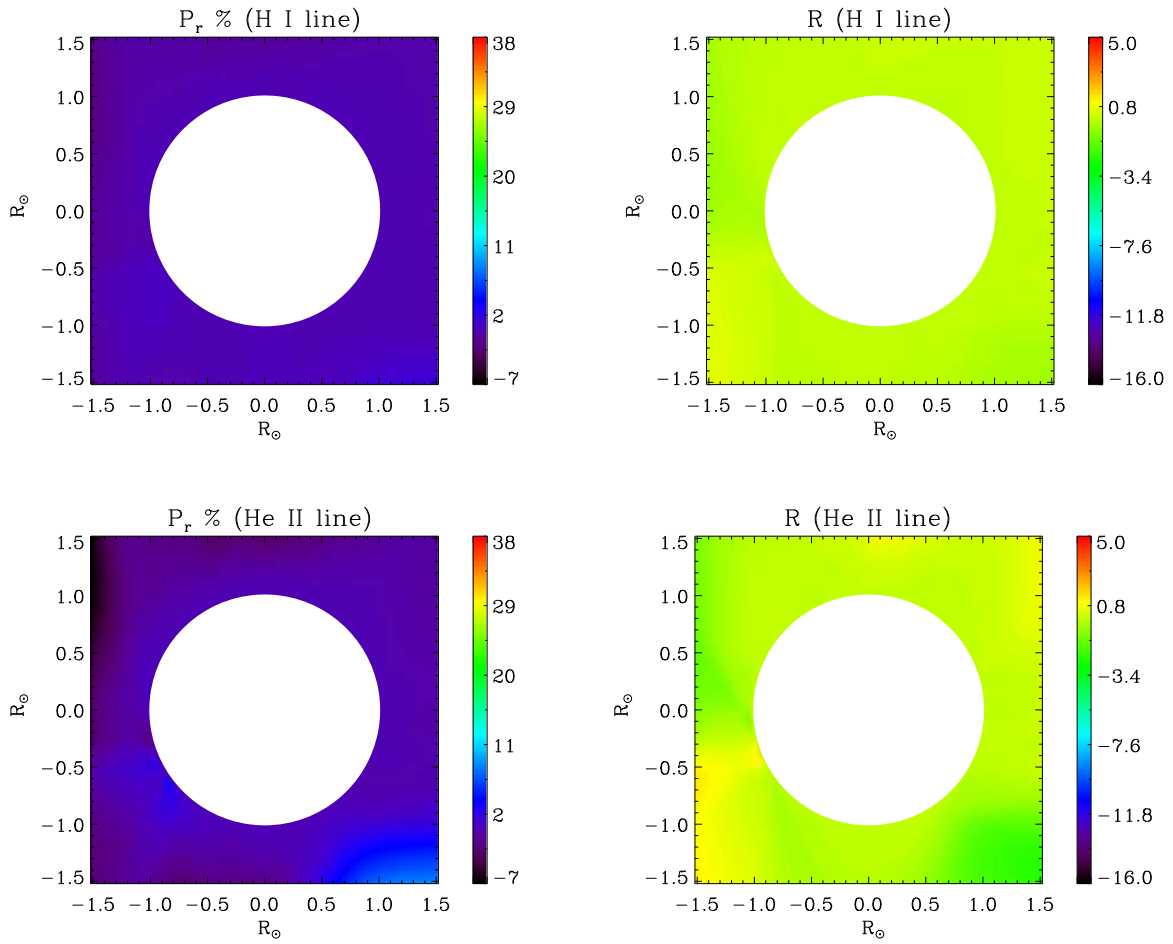


Figure 11. The relative polarization P_r and the rotation angle R of the polarization plane of the Ly α lines of H I (top panels) and the He II (bottom panels) calculated in “the magnetic model” CR2157 ignoring the Hanle effect but taking into account the impact of the model’s macroscopic velocity.

The non-radial solar wind case for various inclinations of the macroscopic velocity is shown in Figure 3 for a height $h = 0.01R_\odot$ above the Sun’s visible disk. It is of interest to note in the four top panels the behavior of J_0^0 and $\sqrt{2}J_1^2/J_0^0$ for non-radial solar winds, which can be understood by arguments similar to those outlined above. For example, for the case of a solar wind velocity perpendicular to the radial direction, the maximum Doppler shift and the corresponding decrease in the intensity seen by the coronal atoms occurs for the radiation beams coming from the sides and directed along the velocity vector. Accordingly, the comoving frame anisotropy factor decreases for the inclination angles 0° – 45° and increases for the later angles. However, they all reach the static value in the limiting case of infinite velocity which is much greater than 1000 km s^{-1} for the representative case in Figure 3. Similar arguments can be made to understand the behavior of the J_1^2 and J_2^2 components, which quantify the breaking of the cylindrical symmetry of the radiation field experienced by the moving coronal atoms. The real components of J_1^2 and J_2^2 are shown in Figure 3. As expected, because of the fulfillment of the cylindrical symmetry, $J_1^2 = J_2^2 = 0$ for $\nu = 0$ and also for the limit of very large velocities ($\gg 1000 \text{ km s}^{-1}$ for the case considered in Figure 3; for such large velocities, the coronal atoms see the far wings of the line radiation coming from the solar disk).

4. Results in 3D Coronal Models from Predictive Science Inc.

In this section we show maps of the frequency-integrated linear polarization signals produced by scattering processes in the Ly α lines of H I and He II, which we have calculated in 3D models of the solar corona. Our aim is to show the different sensitivity of these lines to the model’s magnetic field and macroscopic velocity.

4.1. The 3D Models

We use 3D magneto-hydrodynamic models of the solar corona and inner heliosphere developed by Predictive Science Inc. (see <https://www.predsci.com/portal/home.php>). These publicly available coronal models are developed using photospheric magnetic field observations to specify the boundary condition on the radial component of the magnetic field and they include energy transport processes such as coronal heating, anisotropic thermal conduction, and radiative losses (Lionello et al. 2009; Riley et al. 2015). These 3D models provide the proton number densities, the temperature, the magnetic field, and the velocity of the coronal plasma at each spatial point (in spherical coordinates).

We use two such coronal models: CR2138 (corresponding to 2013 June 30) and CR2157 (corresponding to 2014 November 14). Figures 4 and 5 visualize the temperature, the proton

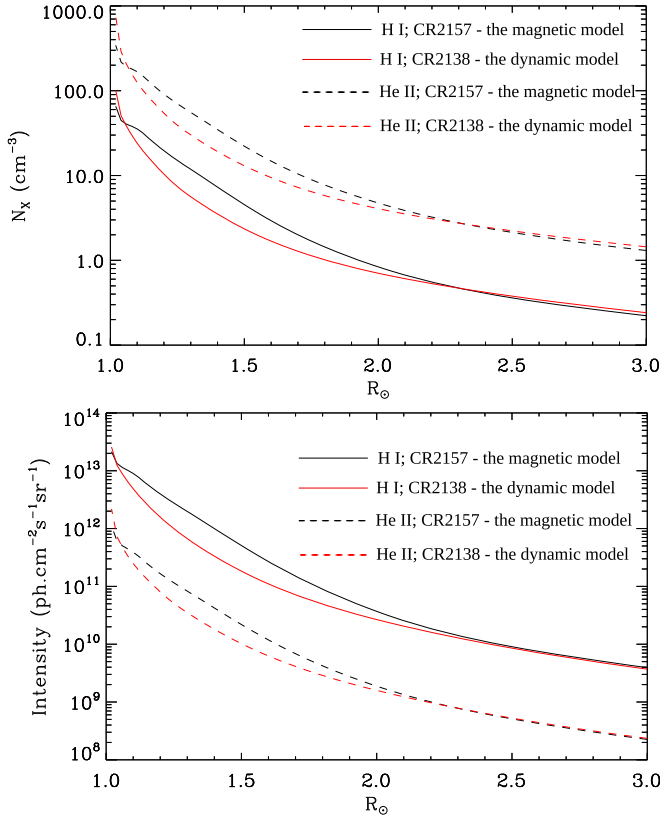


Figure 12. Variation of the model’s number density of H I and He II and of the ensuing Ly α line intensities along the radial direction indicated in Figures 4 and 5. Both these quantities are obtained after the LOS integration.

density, the magnetic field strength and the velocity of models CR2157 and CR2138, respectively. While the model CR2157 shows a close-to-the-limb ($h < 1.5 R_{\odot}$) magnetic activity larger than the model CR2138, it also presents weaker macroscopic velocities at such heights. Hereafter, we call the model CR2157 “the magnetic model” (see Figure 4) and the model CR2138 “the dynamic model” (see Figure 5). These two models are useful to illustrate the different sensitivities of the considered Ly α lines to the coronal magnetic field and to the solar wind velocity. For a better comparison between the two coronal models, Figure 6 shows the variation of the magnetic field strength and modulus of the velocity along the radial directions indicated in the bottom right panels of Figures 4 and 5.

The number densities of H I and He II are computed using the relation

$$N(X^{+m}) = \frac{N(X^{+m})}{N(X)} \frac{N(X)}{N(H)} N(H), \quad (4)$$

where $N(X)$, $N(X^{+m})$, and $N(H)$ are the number density of element X, the number density of element X in the m th ionization stage, and the hydrogen number density, respectively. The ionization fraction of the element X^{+m} , $N(X^{+m})/N(X)$, is taken from the CHIANTI database, version 10 (Dere et al. 1997; Del Zanna et al. 2021). The abundance ratio in the solar corona, $N(X)/N(H)$, is as given in Schmelz et al. (2012). We assume that $N(H)$ is the same as the proton number densities given in the 3D model being considered, i.e., fully ionized plasma.

In the following sections we show:

1. the total number of photons, n_{photons} , emitted per unit area, per unit time, and per steradian;
2. the total linear polarization, $P = \frac{\sqrt{Q^2 + U^2}}{I}$;
3. the relative polarization, $P_r = \frac{P_0 - P}{P_0}$ (with P_0 the degree of polarization when there are no symmetry breaking effects); and
4. the rotation of the polarization plane, $R = \frac{1}{2} \tan^{-1}\left(\frac{U}{Q}\right)$, with respect to the local solar limb.

The linear polarization maps shown below correspond to an LOS integration of $6 R_{\odot}$ centered around the POS.

4.1.1. Polarization Maps of “The Magnetic Model” CR2157

Some physical quantities of this coronal model are shown in Figure 4 for positions in the POS up to approximately two solar radii above the model’s visible disk. The application of our computer code for calculating the polarization of the spectral line radiation scattered by the solar corona allows us to perform several numerical experiments useful for understanding the diagnostic potential of the lines under consideration. We recall that this requires calculating the comoving frame radiation field tensor of the spectral line at each spatial point within the corona of the model, to solve the statistical equilibrium equations to determine the emission coefficient in the Stokes parameters, and to calculate the emergent Stokes signals after integrating along each LOS and over the line’s frequency interval.

We start by considering the nonmagnetized and static case. To this end, we carried out the calculations after forcing to zero the model’s magnetic field and macroscopic velocity. Figure 7 shows the results for the number of photons in the Ly α lines of H I (left panel) and He II (right panel), per unit area, per unit time, and per solid angle unit. In these panels, the overplotted short black lines indicate the direction of the linear polarization signals and their length the polarization amplitude. The number of photons in the line radiation scattered by the model’s corona is larger in the hydrogen Ly α line despite the fact that the number density of residual neutral hydrogen atoms is slightly less than the number density of He II atoms (see the top panel of Figure 12). This is because of the larger incoming radiation for the Ly α line of H I as compared to that of the Ly α line of He II. As seen in the right panel of Figure 7 and the bottom panel of Figure 12, the number of photons in the Ly α line of He II are very low after $0.5 R_{\odot}$ above the model’s visible disk; hence, detecting the polarization of this line at those heights would require prohibitively long integration times and/or telescope apertures. To substantiate this, in Figure 8 we compare the exposure times for both the intensities in Figure 7, needed to measure 10^7 photons with an instrument of 500 cm^2 collection area, $20''$ spatial sampling and an instrument efficiency of 0.01. For this reason, the remaining figures show the results up to $0.5 R_{\odot}$ above the model’s visible disk.

As expected, in the absence of any symmetry breaking, the linear polarization of the scattered radiation is always perpendicular to the solar radius vector through the observed point. Moreover, the amplitude of the linear polarization is the same in both Ly α lines because their levels have the same angular momentum values and, therefore, the same polarizability. This can also be seen in Figure 9, which shows that the total fractional linear polarization signals for the non-magnetic and static case under consideration increase with height in the

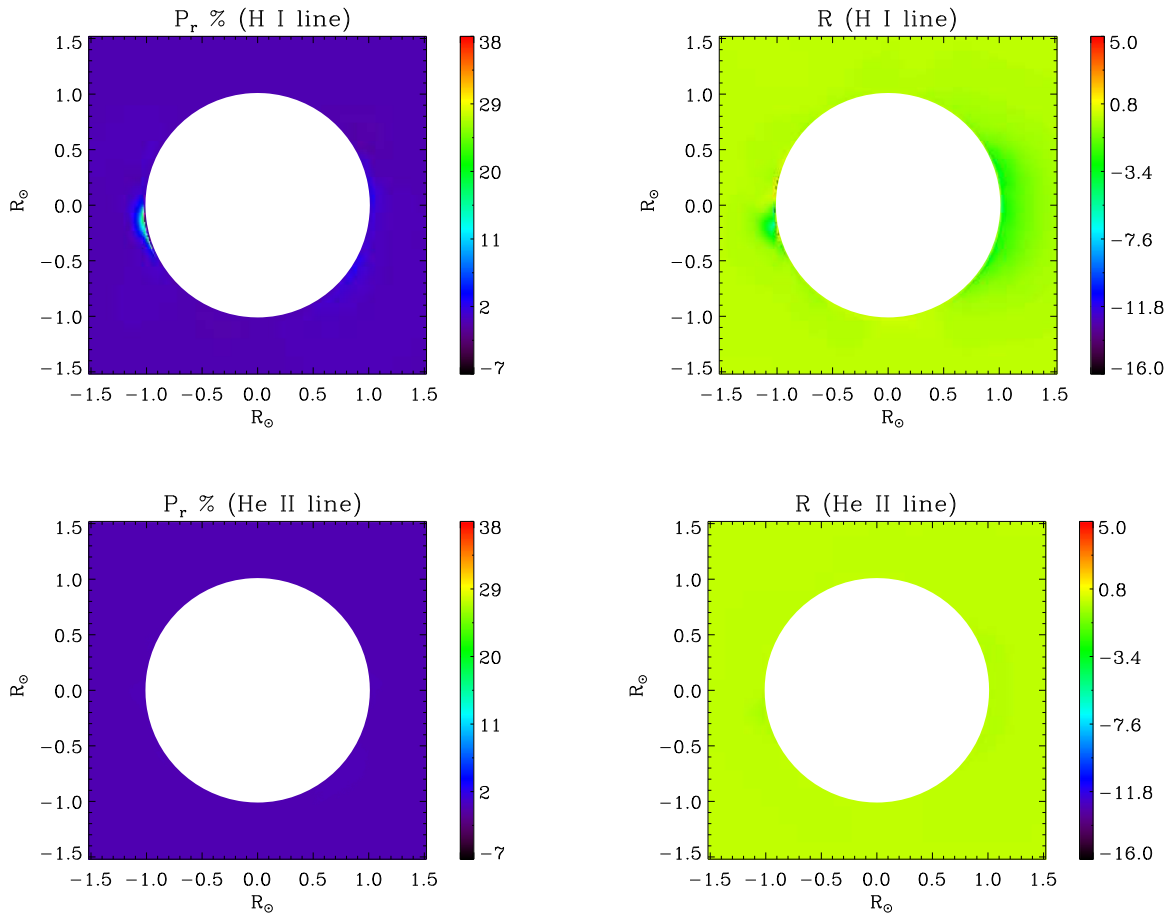


Figure 13. Same as Figure 10 but for “the dynamic model” CR2138.

solar coronal model, reaching values of about 20% at heights $h \approx 0.5R_{\odot}$ above the solar surface.

In Figure 10 we show what happens when we take into account only the Hanle effect produced by the model’s magnetic field (i.e., we force to zero the model’s macroscopic velocity, thus assuming that there is no solar wind). The figure shows the relative polarization P_r (left panels) and the rotation of the polarization plane R for the $\text{Ly}\alpha$ lines of H I (top panels) and He II (bottom panels). Obviously, in the static case being considered $P_r = R = 0$ where the Hanle effect does not operate. As mentioned above, the critical magnetic field for the onset of the Hanle effect is $B_H = 53$ G for the hydrogen $\text{Ly}\alpha$ line and $B_H = 850$ G for the $\text{Ly}\alpha$ line of He II and the typical sensitivity to the Hanle effect occurs for magnetic strengths between $0.2B_H$ and $5B_H$. Given that the magnetic field strengths in “the magnetic model” CR2157 of the solar corona are weaker than 100 G, it is logical to find in Figure 10 that only the hydrogen $\text{Ly}\alpha$ line shows a significant Hanle effect. In particular, in the near-to-the-limb regions where the model’s magnetic field is more intense and/or longitudinal, the Hanle effect in the $\text{Ly}\alpha$ line of H I produces a sizable depolarization and rotation of the polarization plane.

Correspondingly, Figure 11 isolates the impact of the Doppler effect produced by the solar wind of the model (i.e., we force to zero the magnetic field). Because the He II $\text{Ly}\alpha$ line coming from the underlying atmosphere is much narrower than the H I $\text{Ly}\alpha$ line, the impact on the scattering polarization is much more significant for the He II $\text{Ly}\alpha$ line. Nevertheless, since below $1.5R_{\odot}$ the model’s macroscopic velocity is rather

small (see the bottom right panels of Figures 4 and 6), the impact of the model’s solar wind on the linear polarization of the He II line is correspondingly small. In coronal regions similar to those in this model, the He II $\text{Ly}\alpha$ line can be considered to be a useful reference line for facilitating the detection of the fingerprints of the Hanle effect in the hydrogen $\text{Ly}\alpha$ line.

4.1.2. Polarization Maps of “The Dynamic Model” CR2138

As seen in Figure 5, in “the dynamic model” the solar wind velocities are much larger, with values reaching 200 km s^{-1} even at coronal heights lower than $1.5R_{\odot}$ (see also Figure 6). A comparison of the number densities of H I and He II and of their corresponding $\text{Ly}\alpha$ intensities in the two coronal models under consideration are given in Figure 12. The magnetic field of this model is weaker than in “the magnetic model” CR2157 previously considered and thus the impact of the Hanle effect in the $\text{Ly}\alpha$ line of H I is smaller (see the top panels of Figure 13) and there is no hint of the Hanle effect in the $\text{Ly}\alpha$ line of He II (see the bottom panels of Figure 13).

However, the sizable macroscopic velocities of “the dynamic model” wind produce an important depolarization and a rotation of the plane of linear polarization in the He II line (see the bottom panels of Figure 14), much larger than in the broader $\text{Ly}\alpha$ line of H I (see the top panels of Figure 14). Interestingly, the solar wind velocities of “the dynamic model” not only produce a strong depolarization and an anti-clockwise rotation of the polarization plane in the region of the model

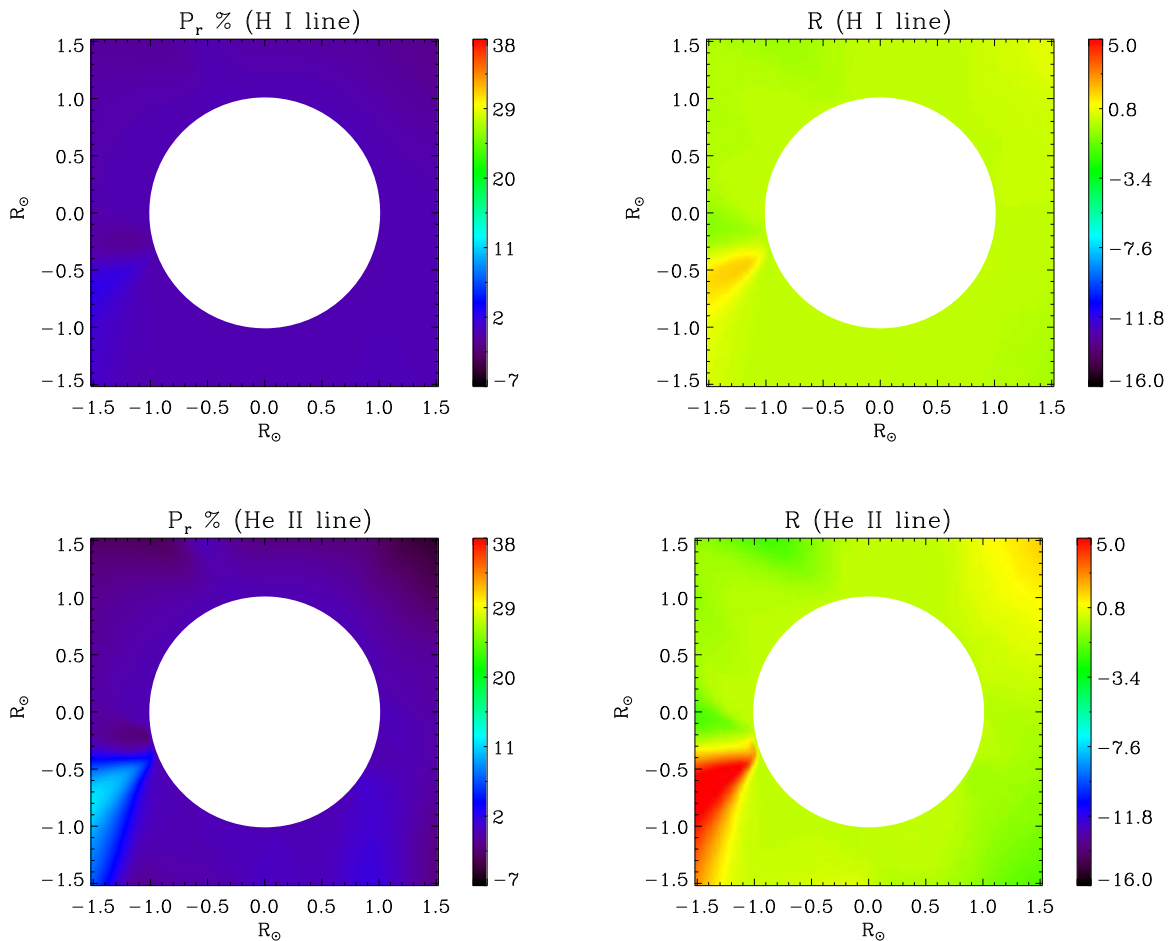


Figure 14. Same as Figure 11 but for “the dynamic model” CR2138.

where the macroscopic velocity is more vigorous, but also an enhancement of the linear polarization and a clockwise rotation of the polarization plane in other regions of the coronal model where the macroscopic velocity is non-radial. In coronal regions similar to those in this model, the hydrogen Ly α line can be considered to be a useful reference line for facilitating the detection of the fingerprints of the solar wind in the Ly α line of He II.

5. Conclusions

The future of coronal spectropolarimetric diagnostics is through spectral lines with complementary sensitivities to the physical quantities of the mega-kelvin plasma. The linear polarization produced by the scattering of anisotropic radiation in suitably chosen spectral lines and its modification by the Hanle effect produced by the magnetic fields of the solar corona is one of the key mechanisms for obtaining empirical information on the solar corona. Here we have considered the Ly α lines of H I and He II investigating their polarization in two 3D coronal models by Predictive Science Inc. The reason for choosing these two lines is their very different sensitivities to the Hanle effect: the critical fields for the onset of the Hanle effect in the Ly α lines of H I and He II being 53 G and 850 G, respectively. Therefore, for the field strengths expected for the solar corona the He II Ly α line is practically insensitive to the Hanle effect, and here we have investigated whether we can use the Ly α line of He II as a reference line for facilitating the

determination of coronal magnetic fields via the Hanle effect in the H I Ly α line.

However, there are other physical mechanisms such as the solar wind velocity, collisions, and active regions on the solar surface that affect the scattering polarization signals generated in the solar corona. Moreover, we have explored the impact of the solar wind velocities on the scattering polarization of the Ly α lines of H I and He II. This is also important because the scattering atoms of H I and He II in the solar corona are irradiated by the spectral line radiation coming from the underlying solar disk, the intensity of which is an emission profile that is broader for the hydrogen Ly α line. Therefore, the coronal atoms see a Doppler-shifted radiation field, which may have a significant impact on the anisotropy and symmetry properties of the radiation field seen by the coronal atoms. We have shown that, while the H I line is mainly sensitive to the Hanle effect, the He II line is mainly sensitive to the solar wind velocities. This is because of the much narrower He II Ly α line coming from the underlying atmosphere as compared to the H I Ly α line. In the present investigation we have assumed that in the solar coronal models the helium abundance is uniform, but in a future investigation we plan to consider the possibility of significant spatial variations in the coronal helium abundance, as indicated by recent suborbital space measurements (Moses et al. 2020).

With the present technology, it should be possible to measure the intensity and polarization signals of both Ly α lines within $0.5 R_{\odot}$ above the Sun’s visible limb, but any measurement above these heights requires much larger integration times. In regions of the solar corona within $0.5 R_{\odot}$ of the solar surface, the solar wind

velocity is usually low and the He II line may be a useful reference line to determine the coronal magnetic field via the Hanle effect in the Ly α line of HI at 1216 Å. However, there might be dynamic events producing high solar wind velocities, even within 0.5 R $_{\odot}$ above the limb. In such cases, the HI Ly α line may be a useful reference line to estimate the solar wind velocities via its effects on the He II Ly α line.

With the new diagnostic tool we have developed we can calculate the Stokes profiles of permitted and forbidden lines that emerge from 3D models of the solar corona and up to heliospheric distances. We are presently extending our theoretical investigations by considering various coronal forbidden lines, such as those to be observed with the Daniel K. Inouye Solar Telescope (DKIST).

We acknowledge the funding received from the European Research Council (ERC) under the European Union's Horizon 2020 Research and Innovation Programme (ERC Advanced grant agreement No. 742265) as well as through the projects PGC2018-095832-B-I00 and PGC2018-102108-B-I00 of the Spanish Ministry of Science, Innovation, and Universities. This research made use of computing time available on the high-performance computing systems of the Instituto de Astrofísica de Canarias and we acknowledge the technical expertise and assistance provided by the Spanish Supercomputing Network. Thanks to the SOLARNET project, which has received funding from the European Union's Horizon 2020 Research and Innovation Programme under grant agreement No. 824135, we obtained computing time at the Piz Daint supercomputer of the Swiss National Supercomputing Centre (CSCS). CHIANTI is a collaborative project involving George Mason University, the University of Michigan (USA), University of Cambridge (UK), and NASA Goddard Space Flight Center (USA).

ORCID iDs

Supriya Hebbur Dayananda  <https://orcid.org/0000-0003-2752-7681>

Javier Trujillo Bueno  <https://orcid.org/0000-0001-5131-4139>

Ángel de Vicente  <https://orcid.org/0000-0002-4930-7754>

Tanausú del Pino Alemán  <https://orcid.org/0000-0003-1465-5692>

References

- Belluzzi, L., Trujillo Bueno, J., & Štěpán, J. 2012, *ApJL*, **755**, L2
 Bommier, V., & Sahal-Brechot, S. 1982, *SoPh*, **78**, 157
 Casini, R. 2005, *PhRvA*, **71**, 062505
 Casini, R., White, S. M., & Judge, P. G. 2017, *SSRv*, **210**, 145
 Cushman, G. W., Farwell, L., Godden, G., & Rense, W. A. 1975, *JGR*, **80**, 482
 Cushman, G. W., & Rense, W. A. 1978, *SoPh*, **58**, 299
 Del Zanna, G., Dere, K. P., Young, P. R., & Landi, E. 2021, *ApJ*, **909**, 38
 Dere, K. P., Landi, E., Mason, H. E., Monsignori Fossi, B. C., & Young, P. R. 1997, *A&AS*, **125**, 149
 Doschek, G. A., Behring, W. E., & Feldman, U. 1974, *ApJL*, **190**, L141
 Favati, B., Landi Degl'Innocenti, E., & Landolfi, M. 1987, *A&A*, **179**, 329
 Fineschi, S., Hoover, R. B., & Walker, A. B. C. J. 1992, *Proc. SPIE*, **1546**, 402
 Fontenla, J. M., Avrett, E. H., & Loeser, R. 1993, *ApJ*, **406**, 319
 Gabriel, A. H., Culhane, J. L., Patchett, B. E., et al. 1995, *AdSpR*, **15**, 63
 Gabriel, A. H., Garton, W. R. S., Goldberg, L., et al. 1971, *ApJ*, **169**, 595
 Khan, A., Belluzzi, L., Landi Degl'Innocenti, E., Fineschi, S., & Romoli, M. 2011, *A&A*, **529**, A12
 Khan, A., & Landi Degl'Innocenti, E. 2012, *A&A*, **543**, A158
 Landi Degl'Innocenti, E., & Landolfi, M. 2004, *Polarization in Spectral Lines (LL04)* (Dordrecht: Kluwer)
 Lionello, R., Linker, J. A., & Mikić, Z. 2009, *ApJ*, **690**, 902
 Moses, J. D., Antonucci, E., Newmark, J., et al. 2020, *NatAs*, **4**, 1134
 Patchett, B. E., Norman, K., Gabriel, A. H., & Culhane, J. L. 1981, *SSRv*, **29**, 431
 Raymond, J. C., Kohl, J. L., Noci, G., et al. 1997, *SoPh*, **175**, 645
 Raouafi, N. E., Riley, P., Gibson, S., et al. 2016, *FrASS*, **3**, 20
 Riley, P., Lionello, R., Linker, J. A., et al. 2015, *ApJ*, **802**, 105
 Sahal-Brechot, S., Bommier, V., & Feautrier, N. 1998, *A&A*, **340**, 579
 Sahal-Brechot, S., Malinovsky, M., & Bommier, V. 1986, *A&A*, **168**, 284
 Schmelz, J. T., Reames, D. V., von Steiger, R., & Basu, S. 2012, *ApJ*, **755**, 33
 Trujillo Bueno, J., Landi Degl'Innocenti, E., & Belluzzi, L. 2017, *SSRv*, **210**, 183
 Trujillo Bueno, J., Štěpán, J., & Belluzzi, L. 2012, *ApJL*, **746**, L9
 Uitenbroek, H. 2001, *ApJ*, **557**, 389
 Warren, H. P., Mariska, J. T., & Wilhelm, K. 1998, *ApJS*, **119**, 105